Energy 221 (2021) 119854

Contents lists available at ScienceDirect

Energy

journal homepage: www.elsevier.com/locate/energy

Entropy and enthalpy changes during adsorption and displacement of shale gas

Kui Lin [a, b], Ya-Pu Zhao [a, b, *]

[a] State Key Laboratory of Nonlinear Mechanics, Institute of Mechanics, Chinese Academy of Sciences, Beijing, 100190, China
[b] School of Engineering Science, University of Chinese Academy of Sciences, Beijing, 100049, China

ARTICLE INFO

Article history:
Received 13 July 2020
Received in revised form
14 December 2020
Accepted 10 January 2021
Available online 13 January 2021

Keywords:
Shale gas
Adsorption/displacement
Entropy change
Enthalpy change
Statistical mechanics

ABSTRACT

Shale gas is a major component of the hydrocarbon economy, and there are abundant studies in related exploration and exploitation fields using simulations and experiments. In this paper, the kinetic processes of adsorption and displacement during shale gas exploitation are analyzed using enthalpy-driven and entropy-driven processes with molecular dynamics simulations and statistical mechanics analyses. First, the changes in symmetry of CH_4 and CO_2 adsorbed on the graphene surface are analyzed. The adsorption process is a spontaneous process, where the Gibbs free energy decreases. During this process, the gas molecular entropy and the enthalpy of the system decrease, which indicates an enthalpy-driven process. The changes in entropy and enthalpy of various gas molecules (CH_4, CO_2, N_2, and H_2O) during the adsorption process are obtained. Through comparing the entropy and enthalpy changes before and after the displacement of CH_4 by the different displacement media (CO_2, N_2, and H_2O). The CO_2-injected displacement of CH_4 is driven by both enthalpy and entropy, and the N_2-injected displacement of CH_4 is driven by entropy. However, H_2O-injected displacement of CH_4 is not a spontaneous process. It plays a certain displacement role by reducing the partial pressure of CH_4. To clarify the detailed spontaneous processes, the entropy change and exothermic processes during the supercritical fluid displacement of shale gas are discussed; then, the differences in displacement efficiency of different supercritical fluids are explained. This study is useful for understanding the kinetics mechanism of adsorption and displacement of shale gas.

1. Introduction

Shale gas is a major component of the hydrocarbon economy and will continue to play a significant role in the future [1,2]. The occurrence state of shale gas mainly includes the free state and the adsorption state [3,4] depending on the pore structure [5] and formation conditions (e.g., pressure and temperature) [6]. However, the storage characteristics of shale gas are complicated as a result of changes in stratigraphic structure. In addition, it is difficult for one mining method to be effectively applied to all storage conditions (e.g. the pore size [7], apparent permeability [8], and depth [9,10]). Heller et al. [11] measured the adsorptive capacity of four gas shale samples and found the differences. Hence, understanding the adsorption mechanism of shale gas in the shale matrix is a prerequisite for establishing a model to quantitatively evaluate the amount of gas adsorbed/desorbed under different geological conditions. Researchers can calculate macroscopic variables and phenomena, such as the adsorptive capacity, adsorptive heat [12], crossover of excess adsorption isotherms [13], diffusion in shale [14], transport in micro/nanoporous [15,16], and pyrolysis of kerogen [17,18] using microscale methods, such as the grand canonical Monte Carlo (GCMC) and molecular dynamics (MD) methods. The matrix of shale is mainly composed of inorganic and organic matter, including clay minerals, montmorillonite, illite, chlorite, kaolinite, quartz, calcite and pyrite. Yang [19] and Wang [20] et al. studied the adsorption behavior of CO_2, CH_4 and their mixture in montmorillonite clay. The negative electrons on the clay surface and sodium ions between layers could enhance the adsorption of CO_2 molecules on the matrix [21]. Because of the competition of adsorption sites among H_2O, CH_4, and CO_2 molecules, the presence of H_2O inevitably reduces the adsorption capacity of CH_4/CO_2 on sodium-, cesium-, calcium-montmorillonite clay [22]. Huang and Zhao first explored the mechanism of

* Corresponding author. State Key Laboratory of Nonlinear Mechanics, Institute of Mechanics, Chinese Academy of Sciences, Beijing, 100190, China.
E-mail address: yzhao@imech.ac.cn (Y.-P. Zhao).

https://doi.org/10.1016/j.energy.2021.119854
0360-5442/

adsorption blockage caused by the interaction between supercritical CO_2 and nanopores through experiments [23]. They clarified that the blockage was caused by the interaction of supercritical CO_2 and physisorption, association adsorption and dissociation adsorption of shale pores. In addition, Feng et al. [24] investigated the effect of supercritical CO_2 adsorption on the failure behavior of shale and found that fragmentation was the root cause of deterioration in the mechanical properties of shale.

Shale gas contains a large amount of adsorbed gas (20%~80%); thus, gas desorption is one of the most important processes during exploitation. For the shale gas in mesopores and macropores, high recovery can be achieved by direct decompression. However, for shale gas in micropores, displacement becomes a more efficient choice. Displacement refers to the transformation of shale gas from the adsorbed state to the free state or the displacement of shale gas from the confined pore (including the adsorbed state and free state) to the main channel to achieve exploitation, as shown in Fig. 1. Therefore, some researchers proposed using CO_2 to displace adsorbed CH_4 [25,26]. Shi et al. [27] proposed a bidisperse pore diffusion model for CH_4 displacement desorption by CO_2 injection. Yuan and Zhao [28] were the first to study the displacement process of confined CH_4 by injecting CO_2 into the pore structure by MD simulation. The simulation results show that the CO_2 injection method can increase recovery by at least 15% compared to the depressurization method. Wu et al. [29] studied the displacement process of CH_4 in slits by injecting CO_2 and N_2. They found that both CO_2 and N_2 injection could increase recovery, but the physical mechanism is different. CO_2 can directly displace CH_4, while N_2 can increase recovery by reducing the partial pressure of CH_4. Liang et al. [30] investigated the displacement of CH_4 in a coal seam by injecting CO_2 through experiments and found that CO_2 had a stronger adsorption capacity than CH_4 during the displacement process. Zhang et al. performed the surface modification of inorganic clay mineral surface-modified organic matter and then simulated the displacement of CH_4 by CO_2 [31]. Lin et al. compared the displacement barriers injected with different gas molecules (CO_2, N_2, and H_2O) and displacement efficiency of confined CH_4 with various supercritical fluids by MD simulation. The results show that the displacement efficiency is in the order of $CO_2 > N_2 > H_2O$ [32].

Previous studies mostly focused on the phenomenological analysis or qualitative analysis of shale gas adsorption and displacement processes by simulation or experiment. However, there has been no study on the mechanism of entropy-driven and enthalpy-driven processes of adsorption and displacement. In this paper, the enthalpy and entropy changes during the process of adsorption and displacement are analyzed from the thermodynamic entropy and enthalpy criterion. First, the degrees of freedom before and after adsorption and the displacement of several commonly used displacement media (CO_2, N_2, and H_2O) and CH_4 are analyzed. The entropy changes before and after adsorption and displacement are calculated by analyzing the changes in translational and rotational entropy of molecules. Through the calculation and analysis of the enthalpy and entropy changes that occur during the displacement of CH_4 by different displacement media, the changes in the Gibbs free energy are obtained. The enthalpy-driven, entropy-driven, dual-driven, spontaneous process and nonspontaneous process changes during the displacement process of different displacement media are clarified. This study provides a new idea to explain the displacement efficiency of shale gas that has been displaced by different supercritical fluids and deepens the understanding of adsorption and displacement kinetics mechanisms in confined spaces.

2. Problem formulation and research approach

2.1. Thermodynamic process of gas adsorption

Whether a thermodynamic process is spontaneous depends on the Gibbs free energy of the system, where the Gibbs free energy expression is:

$$\Delta G = \Delta H - T\Delta S \tag{1}$$

where H is the enthalpy, S is the entropy and T is the absolute temperature. If the process reduces the free energy of the system, the process is spontaneous. From the formula, the process is spontaneous when enthalpy decreases and entropy increases. When enthalpy increases, there is a decrease in entropy, and the process is not spontaneous; when enthalpy decreases, entropy decreases, or enthalpy increases and entropy increases, and a specific calculation is required to determine whether the process is spontaneous.

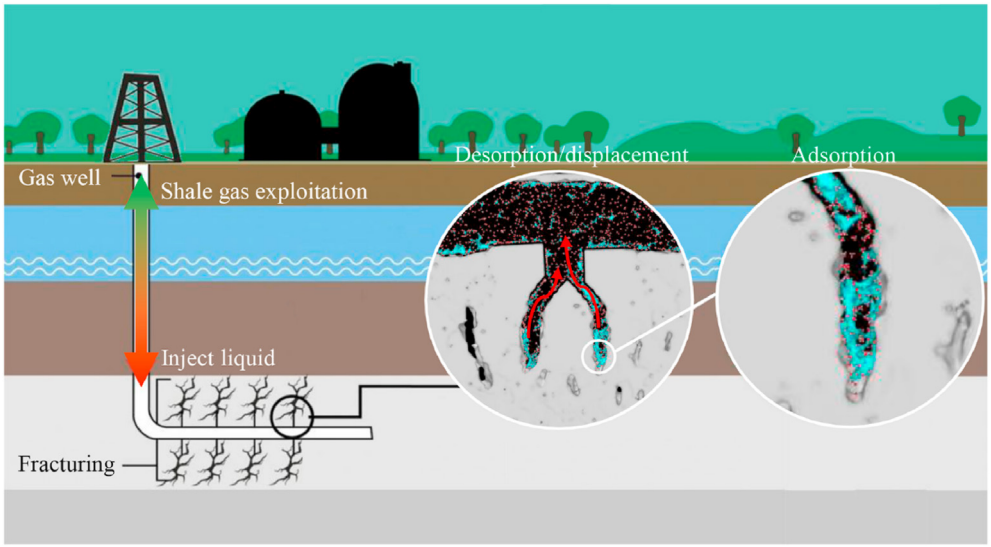

Fig. 1. Schematic of desorption and displacement in shale gas exploitation.

Adsorption can be divided into physisorption and chemisorption according to the different force attributes of adsorption. The mechanism of physisorption is through van der Waals force action. When molecules are sufficiently close, there will be van der Waals force action, so physisorption is not selective. The mechanism of chemisorption is through the formation of chemical bonds, so chemisorption has selectivity. van der Waals forces are weaker than chemical bonds; thus, physisorption is unstable, and desorption easily occurs. Chemisorption is stable, and desorption does not easily occur. Physisorption is the main form of adsorption in shale gas systems, which makes it possible to exploit shale gas.

In the natural state, the adsorption process is a spontaneous process that reduces the Gibbs free energy. This process corresponds to decreases in enthalpy and entropy, and it is an enthalpy-driven process. For the displacement process, if the molecule can spontaneously displace another adsorbed molecule, the displacement process must be a process of decreasing Gibbs free energy. To explore the best displacement medium and displacement thermodynamics of shale gas, the change in entropy during the process of molecular adsorption and displacement from the perspective of thermodynamic entropy should be analyzed. Therefore, this paper mainly analyzes the entropy change and enthalpy change in the process of adsorption and displacement and determines whether the entire process is spontaneous through equation (1). If it is spontaneous, we then determine whether it is driven by enthalpy or entropy.

2.2. Space group of molecules and adsorption-induced symmetry breaking

This section analyzes the change in symmetry of CH_4 adsorbed on the graphene surface. The CH_4 molecule has a tetrahedral structure that can be analyzed in a cube, and its space group has 24 orders, which are expressed as:

$$T_d = \{E, 3C_2, 8C_3, 6S_4, 6\sigma_d\}. \tag{2}$$

It consists of three two-axis C_2 and four triple-axis C_3, rotating around the three axes $\pi/2$ and $3\pi/2$ of the cube, then mirroring the horizontal plane, and there are six symmetrical operations $6S_4$, mirroring the section formed by the diagonal of the opposite cube, there are six symmetrical operations $6\sigma_d$.

The CO_2 molecule is a linear central symmetric molecule with a space group with two infinite axes ∞C_2, one infinite axis C_∞, an infinite number of mirrors $\infty\sigma$ (σ_h, $\infty\sigma_v$), and an inversion i as follows:

$$D_{\infty h} = \{E, C_\infty, \infty C_2, \infty\sigma, i\}. \tag{3}$$

Graphene has a hexagonal two-dimensional structure, the point group is D_{6h}, and its subgroups contain C_s, C_i, C_2, C_3, C_6, D_2, D_3, D_6, C_{2v}, C_{3v}, C_{6v}, C_{2h}, C_{3h}, C_{6h}, D_{2h}, D_{3h}, D_{3d}, and S_6. Among them, the high-symmetry points of the top, bridge, and hollow correspond to subgroups C_3, C_2, and C_6, and their orders are 3, 2, and 6, respectively.

For the adsorption symmetry of CH_4 on graphene, because C_2 and C_3 are subgroups of T_d and subgroups of C_6, to maximize the adsorption symmetry and because the highest-order group after adsorption is triple-symmetry C_3, the CH_4 axis must be perpendicular to the top or hollow site of graphene. When graphene (or CH_4) remains stationary after adsorption at a designated site, CH_4 (or graphene) can form two adsorption configurations with the C_3 rotating groups. There are two choices for hydrogen atoms, up or down, at each highly symmetric position; thus, there are $2\times 2\times 2 = 8$ adsorption configurations that must be calculated, as shown in the positions of the blue, yellow, red and green blocks in Fig. 2 (c).

For CO_2, its subgroup C_2 is first considered, while the rotational group of vertical graphene passing through the bridge is C_2, and its subgroup at the hollow position contains C_2. Therefore, two C_2 axes can be formed at the bridge and hollow positions. Since CO_2 also contains subgroup C_∞, it can form six-fold symmetry with graphene, i.e., group C_6 at the hollow site, with only one adsorption configuration, as shown in Fig. 2 (d) for Case 3. Therefore, there are five types of computational configurations for CO_2.

From the above analysis, regardless of which molecule is adsorbed by any adsorption configuration, the symmetry of graphene is broken. These analyses use graphene as the adsorbent; thus, the symmetry changes that occur before and after the adsorption gas can be clearly analyzed. The above analysis is for the high-symmetry site, which is determined by calculating and comparing the binding energy of the ideal adsorption configuration. However, in the actual adsorption of the graphene surface, the adsorption of molecules does not strictly adhere to the ideal adsorption site. For the physical adsorption of the graphene surface, the difference in binding energy between different sites is very small, and the adsorption of each molecule will change the potential energy distribution of the original surface. Thus, the gas adsorption is basically evenly distributed on the graphene surface. Fig. 2 in Ref. [28] shows the distribution of CH_4 and CO_2 on the graphene surface.

For actual shale surfaces, the structure and composition are much more complex than graphene or any single component structure, but it is confirmed that most shale gas is physically adsorbed. To simplify the analysis, the shale base as an ideal homogeneous surface with considerable adsorption potential can be imagined. There is no need to consider the symmetry of the substrate for the adsorption of gas on a uniform surface, since each point on the substrate has an infinite axis C_∞ and the entire surface has an infinite number of sites, i.e., ∞C_∞. Therefore, only the change in the degrees of freedom of gas molecules before and after adsorption must be analyzed to determine the change in configuration entropy.

2.3. Molecular degrees of freedom

Molecular degrees of freedom are the basis for calculating the entropy of the molecular configuration. This section gives a brief introduction to molecular degrees of freedom and analyzes the changes in the molecular degrees of freedom during adsorption and displacement.

The degree of freedom is the number of independent coordinates that can be written in the motion equation of an object. The motion of a molecule includes translation, rotation, and vibration. Translation refers to the change in position of the center of the molecule mass in space, rotation refers to the change in the orientation of the molecule in space, and vibration refers to the change in the relative position of the atoms in the molecule. For molecules whose temperatures are far below the characteristic temperature of the molecular vibration, the vibration degree of freedom can be neglected, resulting in a rigid molecule; that is, only the translational and rotational degrees of freedom should be considered.

2.4. Molecular entropy

A statistical expression based on the ideal gas entropy function is as follows:

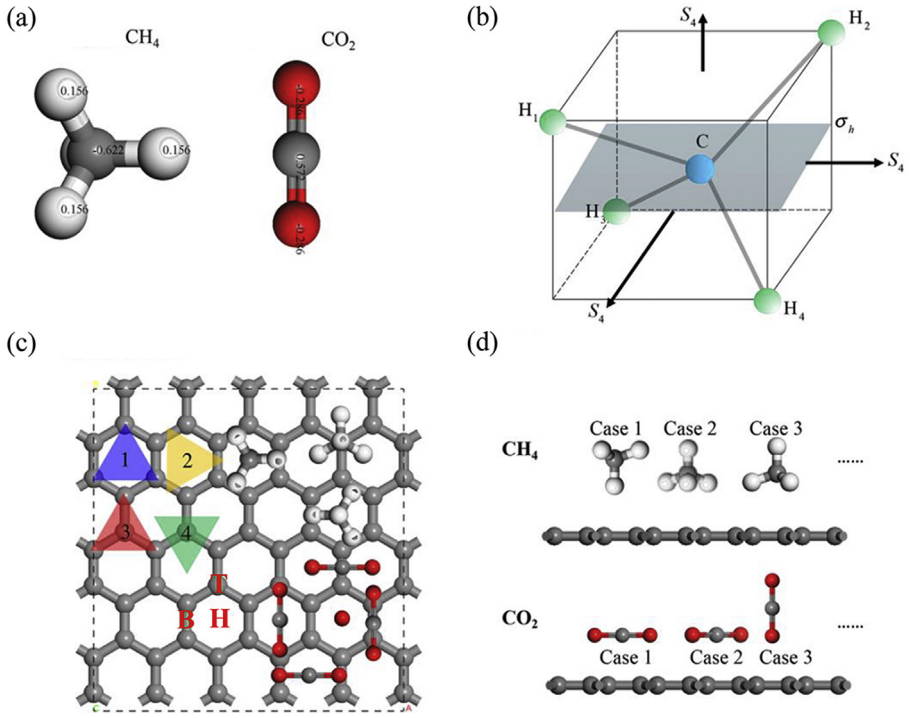

Fig. 2. Space point group and density functional theory (DFT) calculation model of molecular adsorption on graphene. (a) CH_4, CO_2. (b) Space point group of CH_4. (c) High-symmetry adsorption site: Top (T), Bridge (B), Hollow (H). (d) Adsorption configuration.

$$S = Nk_B\left(\ln Z_1 - \beta\frac{\partial}{\partial\beta}\ln Z_1\right) - k_B \ln N!, \tag{4}$$

where N is the number of particles, k_B is the Boltzmann constant, $\beta = 1/k_BT$, and Z_1 is the partition function of a single atomic molecule:

$$Z_1 = V\left(\frac{2\pi m}{h^2\beta}\right)^{3/2}, \tag{5}$$

where m is the relative molecular mass and h is Planck's constant. Substituting equation (5) into equation (4) and combining the approximation $\ln N! = N(\ln N - 1)$ to obtain the entropy of the monoatomic ideal gas yield:

$$S = \frac{3}{2}Nk_B \ln T + Nk_B \ln\frac{V}{N} + \frac{3}{2}Nk_B\left[\frac{5}{3} + \ln\left(\frac{2\pi mk_B}{h^2}\right)\right]. \tag{6}$$

For the rotation entropy, there is a rotational partition function according to the corresponding three rotation axes in the three-dimensional space. When there is only one rotation axis, the rotation partition function is:

$$q_1^r = \pi^{\frac{1}{2}}\left(\frac{8\pi^2k_BT}{h^2}\right)^{\frac{1}{2}}I_1^{\frac{1}{2}}. \tag{7}$$

The moment of inertia I_1 is:

$$I_1 = \sum_i m_i\left(x_i^2 + y_i^2\right). \tag{8}$$

When there are two axes of rotation, the rotation partition function is:

$$q_2^r = \left(\frac{8\pi^2k_BT}{h^2}\right)I_2. \tag{9}$$

The moment of inertia I_2 is:

$$I_2 = \left\{\left[\sum_i m_i\left(x_i^2 + y_i^2\right)\right]\left[\sum_i m_i\left(y_i^2 + z_i^2\right)\right]\right\}^{\frac{1}{2}}. \tag{10}$$

When there are three axes of rotation, the rotation partition function is:

$$q_3^r = \pi^{\frac{1}{2}}\left(\frac{8\pi^2k_BT}{h^2}\right)^{\frac{3}{2}}I_3^{\frac{1}{2}}. \tag{11}$$

The moment of inertia I_3 is:

$$I_3 = I_aI_bI_c = \begin{vmatrix} I_{xx} & -I_{xy} & -I_{xz} \\ -I_{xy} & I_{yy} & -I_{yz} \\ -I_{xz} & -I_{yz} & I_{zz} \end{vmatrix}. \tag{12}$$

The expression of the rotation entropy is:

$$S_n^r = N_Ak_B\left(\frac{n}{2} + \ln q_n^r\right), \tag{13}$$

where n is the number of independent axes of rotation; for a free linear molecule $n = 2$, and for a free nonlinear molecule $n = 3$. More details on the formulas of rotational entropy can be found in Ref. [33].

3. Results and discussion

3.1. Changes in molecular degrees of freedom during adsorption and displacement

The degree of freedom of molecular translation includes three independent targets in space, so the translational freedom of a single molecule is 3. The degree of rotational freedom is divided between linear and nonlinear molecules. Linear molecules are composed of atoms all along a straight line, such as CO_2 and N_2. As shown in Fig. 3, the spatial orientation of the linear molecules is determined by precession and chapter; thus, there are 2 degrees of rotational freedom. Nonlinear molecules are those in which the atoms are not oriented in a straight line, such as H_2O. As shown in Fig. 3, the spatial orientation of nonlinear molecules is determined by precession, chapter and rotation; thus, there are 3 rotational degrees of freedom.

The vibrational freedom of N atom molecules is the total number of degrees of freedom (3 N) minus the translational degrees of freedom and rotational degrees of freedom. The calculations of various degrees of freedom of the molecules are shown in Table 1. The changes in molecular degrees of freedom during adsorption and displacement are based on the following assumptions: (1) the molecules studied in this paper are rigid molecules, (2) the substrate is homogeneous and isotropic, and (3) the molecular idealization for the adsorption state is considered a rigid constraint in the Z direction. As shown in Fig. 3 (c) and (d), taking the CO_2 displacing CH_4 as an example, the degree of freedom for CO_2 in the displacement process changes from 5 degrees of freedom (free state) to 3 degrees of freedom (adsorption state), and CH_4 is changed from 3 degrees of freedom (adsorption state) to 6 degrees of freedom (free state). H_2O and N_2 have 6 degrees of freedom and 5 degrees of freedom before displacement, respectively. After displacement, these molecules have 3 degrees of freedom, which include 2 translational degrees of freedom and 1 rotational degree of freedom.

Table 1
Molecular degrees of freedom.

Molecular type	Translation	Rotational	Vibrational	Total
Monatomic	3	0	0	3
Linear	3	2	$3N-5$	$3N$
Non-linear	3	3	$3N-6$	$3N$

3.2. Calculation of the configuration entropy during adsorption and displacement

The equation of state for an ideal gas is:

$$p = \frac{N}{\beta}\frac{\partial}{\partial V}\ln Z_1 = \frac{Nk_BT}{V} \tag{14}$$

Since equation (6) is the entropy of a monoatomic ideal gas and the monoatomic ideal gas has only 3 translational degrees of freedom, equation (6) can be applied to calculate the translational entropy of any ideal gas. Therefore, combining equations (6) and (14), the translational entropy of 1 mol of molecular gas is:

$$S^t_{(g)} = N_Ak_B\ln\frac{(2\pi mk_BT)^{\frac{3}{2}}k_BT}{h^3p} + \frac{5}{2}N_Ak_B, \tag{15}$$

where N_A is the Avogadro constant.

For the adsorbed gas, there are only two translational degrees of freedom, and the translational entropy of 1 mol of adsorbed gas is:

$$S^t_{(a)} = N_Ak_B\ln\frac{(2\pi mk_BT)k_BT}{h^2p'} + 2N_Ak_B, \tag{16}$$

where p' is the pressure at which the adsorbed gas is located. The translational entropy change of the gas molecules from the ideal state to the adsorbed state becomes:

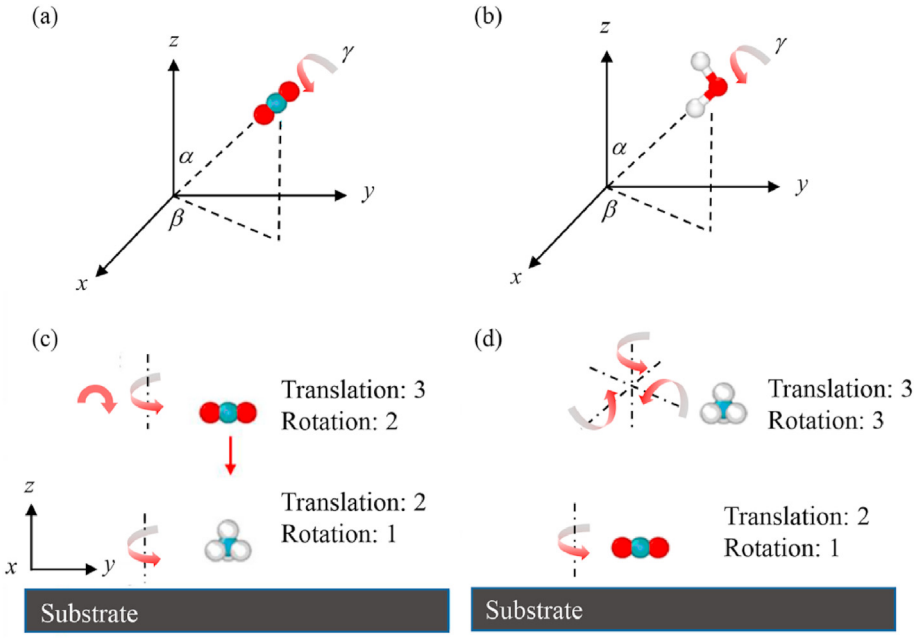

Fig. 3. Molecular degrees of freedom. (a) Linear molecules. (b) Nonlinear molecules. (c) Before displacement. (d) After displacement.

$$\Delta S^{t} = S^{t}_{(a)}(p') - S^{t}_{(g)}(p) = -N_A k_B \ln\frac{(2\pi m k_B T)^{1/2} p'}{hp} + \frac{N_A k_B}{2}. \quad (17)$$

According to equation (17), the translational entropy change can be calculated as shown in Table 2. The entropy change discussed in this section is an ideal state or a maximum entropy change, i.e., the entropy change between equilibrium states.

For linear molecules (CO_2 and N_2), the process is from the free state with two rotational degrees of freedom to the adsorbed state with one rotational degree of freedom. Therefore, combining equations (7), (9) and (13), the rotational entropy change becomes:

$$\Delta S^{r} = S^{r}_{1} - S^{r}_{2} = -N_A k_B \left\{ \frac{1}{2} + \ln\left[\left(\frac{8\pi k_B T}{h^2}\right)^{\frac{1}{2}} \frac{I_2}{I_1^{\frac{1}{2}}} \right] \right\}. \quad (18)$$

For nonlinear molecules (CH_4 and H_2O), the process is from the free state with three rotational degrees of freedom to the adsorbed state with one rotational degree of freedom. Therefore, combining equations (7), (11) and (13), the rotational entropy change becomes:

$$\Delta S^{r} = S^{r}_{1} - S^{r}_{3} = -N_A k_B \left\{ 1 + \ln\left[\left(\frac{8\pi^2 k_B T}{h^2}\right) \frac{I_3^{\frac{1}{2}}}{I_1^{\frac{1}{2}}} \right] \right\}. \quad (19)$$

For each molecule, the calculation of the rotational entropy change from the free state to the adsorption state is shown in Table 3.

For the displacement process, CO_2 drives CH_4, and the rotational entropy increases by 42.18 J mol^{-1} K^{-1}; in addition, N_2 drives CH_4, and the rotational entropy increases by 41.55 J mol^{-1} K^{-1}, while the H_2O displacement reduces the rotational entropy by 5.47 J mol^{-1} K^{-1}. Combining translational and rotational entropy changes, the entropy changes of adsorbed CH_4 displaced by different displacement media can be obtained, as shown in Table 4. Therefore, both CO_2 and N_2 displacing CH_4 are entropy-increasing processes, and H_2O displacing CH_4 is an entropy-decreasing process.

3.3. Enthalpy and free energy changes of the CH_4 displacement by different molecules

Without external work, the change in internal energy of the system is equal to the change in enthalpy. The energy changes of CH_4, CO_2, H_2O, and N_2 on the surface of graphene are studied in detail in Ref. [32]. The corresponding adsorption energies are shown in Table 5. Therefore, for an ideal displacement process, the enthalpy changes of the adsorbed CH_4 when CO_2, H_2O, and N_2 are used as the displacement medium are shown in Table 6. From the changes in enthalpy, the CO_2-injected displacement of CH_4 is an exothermic process, while the H_2O-injected and N_2-injected displacement of CH_4 are endothermic processes.

According to equation (1), the Gibbs free energy changes (at 300 K) of the system during the ideal displacement can be obtained by combining the enthalpy changes of various molecular displacements in Table 5 and the entropy changes of molecular displacements in Tables 2 and 3. The Gibbs free energy changes of CH_4 displacement by injecting CO_2, H_2O and N_2 are −19.72 kJ/mol, 15.57 kJ/mol, and −11.39 kJ/mol, respectively. Therefore, the CO_2-injected and N_2-injected displacement of CH_4 show an increase in entropy, and they are spontaneous processes; in addition, the CO_2-injected displacement of CH_4 is driven by both enthalpy and entropy, and the N_2-injected displacement of CH_4 is driven by entropy. However, H_2O-injected displacement of CH_4 is not a spontaneous process. It plays a certain displacement role by reducing the partial pressure of CH_4. Hence, the differences in displacement efficiency of different supercritical fluids (CO_2 > N_2 > H_2O) can also be explained by statistical mechanics and thermodynamics analysis. It is useful for understanding the kinetics mechanism of adsorption and displacement of shale gas from a new perspective.

Table 2
The translational entropy changes of molecules displace CH_4.

displacing medium	CO_2	H_2O	N_2
ΔS^t(J · mol^{-1} K^{-1})	−3.01	−0.36	−1.69

Table 3
Rotational entropy changes of molecules.

	CH_4	CO_2	H_2O	N_2
I_1(10^{-43}g·m^2)	0.5389	7.2350	1.1614	8.4387
I_2(10^{-43}g·m^2)	0	7.2350	0	8.4387
I_3(10^{-129}g^3·m^6)	0.1565	0	1.2560	0
ΔS^r(J·mol^{-1}·K^{-1})	− 96.44	− 54.26	− 101.91	− 54.89

Table 4
Entropy change of CH_4 displacement by different molecules.

Displacing medium	**CO_2**	**H_2O**	**N_2**
ΔS^t(J·mol^{-1} K^{-1})	−3.01	−0.36	−1.69
ΔS^r(J·mol^{-1} K^{-1})	42.18	−5.47	41.55
ΔS(J·mol^{-1} K^{-1})	39.17	−5.83	39.86

Table 5
Adsorption energies of CH_4, CO_2, H_2O and N_2 on graphene [32].

Adsorbate	E_{ad} (kJ/mol)
CH_4	−24.32
CO_2	−32.27
H_2O	−10.46
N_2	−23.73

Table 6
Enthalpy change of CH_4 displacement by different molecules.

Displacing medium	CO_2	H_2O	N_2
ΔH (kJ/mol)	−7.95	13.85	0.59

4. Conclusions

First, the adsorption of several commonly used displacement media (CO_2, N_2, and H_2O) and CH_4 are analyzed in addition to the degrees of freedom before and after the displacement. By analyzing the translational and rotational entropy changes of the molecule, the entropy is calculated before and after the molecular adsorption and displacement. When CO_2 displaces CH_4, the entropy increases by 39.17 J·mol^{-1}·K^{-1}; when N_2 displaces CH_4, the entropy increases by 39.86 J·mol^{-1}·K^{-1}; and when H_2O displaces CH_4, entropy decreases by 5.83 J·mol^{-1}·K^{-1}. An analysis of the enthalpy changes during the displacement of CH_4 by different displacement media shows that the CO_2-injected displacement of CH_4 is an exothermic process with decreasing enthalpy, and the displacements of CH_4 by H_2O and N_2 are endothermic processes of increasing enthalpy. Combining the enthalpy change and entropy

change, the Gibbs free energy change (at 300 K) of the system can be obtained during the ideal displacement. The Gibbs free energy changes of the CH_4 displacement by CO_2, H_2O, and N_2 are −19.72 kJ/mol, 15.57 kJ/mol, and −11.39 kJ/mol, respectively. Therefore, the CO_2-injected and N_2-injected displacements of CH_4 are processes of increasing entropy, and they are spontaneous. The CO_2-inected displacement of CH_4 is an enthalpy and entropy dual-driven process, the N_2-injected displacement of CH_4 is entropy-driven process, and the H_2O-injected displacement of CH_4 is a nonspontaneous and endothermic process. Although the processes in engineering application are often far from equilibrium, the research in this article provides a new perspective to explain the displacement efficiency of different supercritical fluids in displacing shale gas, and it deepens the understanding of the adsorption and displacement kinetic mechanism of shale gas. The results can be useful for exploitation of shale gas field.

Credit author statement

Kui Lin: Methodology, Analysis, Writing – original draft, Editing. Ya-Pu Zhao: Methodology, Writing – review & editing, Supervision, Project administration.

Declaration of competing interest

The authors declare that they have no known competing financial interests or personal relationships that could have appeared to influence the work reported in this paper.

Acknowledgments

This work was jointly supported by the National Natural Science Foundation of China (NSFC, Grant No. 12032019, 11872363, 51861145314), the Chinese Academy of Sciences (CAS) Key Research Program of Frontier Sciences (Grant No. QYZDJ-SSW-JSC019), and the CAS Strategic Priority Research Program (Grant No. XDB22040401).

References

[1] Tomain JP. Shale gas and clean energy policy. Case West Reserv Law Rev 2012;63:1187.
[2] Hughes JD. Energy: a reality check on the shale revolution. Nature 2013;494:307–8.
[3] Ross DJ, Bustin RM. Shale gas potential of the lower Jurassic Gordondale member, northeastern British Columbia, Canada. Bull Can Petrol Geol 2007;55:51–75.
[4] Das J. Extracting natural gas through desorption in shale reservoirs. Way 2012;8:11–3.
[5] Zeng W-T, Zhang J-C, Ding W-L, Wang X, Zhu D, Liu Z. The gas content of continental Yanchang shale and its main controlling factors: a case study of Liuping-171 well in Ordos Basin. Nat Gas Geosci 2014;25:291–301.
[6] Zhu H, Ju Y, Huang C, Chen F, Chen B, Yu K. Microcosmic gas adsorption mechanism on clay-organic nanocomposites in a marine shale. Energy 2020;197:117256.
[7] Al Hinai A, Rezaee R, Esteban L, Labani M. Comparisons of pore size distribution: a case from the Western Australian gas shale formations. J Unconvent Oil and Gas Resour 2014;8:1–13.
[8] Javadpour F. Nanopores and apparent permeability of gas flow in mudrocks (shales and siltstone). J Can Petrol Technol 2009;48:16–21.
[9] Wang H, Li G, Shen Z. A feasibility analysis on shale gas exploitation with supercritical carbon dioxide. Energy Sources, Part A Recovery, Util Environ Eff 2012;34:1426–35.
[10] Sun WJ, Feng YY, Jiang CF, Chu W. Fractal characterization and methane adsorption features of coal particles taken from shallow and deep coalmine layers. Fuel 2015;155:7–13.
[11] Heller R, Zoback M. Adsorption of methane and carbon dioxide on gas shale and pure mineral samples. J Unconvent Oil and Gas Resour 2014;8:14–24.
[12] Lin K, Yuan Q, Zhao Y-P. Using graphene to simplify the adsorption of methane on shale in MD simulations. Comput Mater Sci 2017;133:99–107.
[13] Lin K, Huang X, Zhao Y-P. Combining image recognition and simulation to reproduce the adsorption/desorption behaviors of shale gas. Energy Fuels 2020;34:258–69.
[14] Wang H, Qu Z, Yin Y, Bai J, Yu B. Review of molecular simulation method for gas adsorption/desorption and diffusion in shale matrix. J Therm Sci 2019;28:1–16.
[15] Yu H, Zhu Y, Jin X, Liu H, Wu H. Multiscale simulations of shale gas transport in micro/nano-porous shale matrix considering pore structure influence. J Nat Gas Sci Eng 2019;64:28–40.
[16] Zhu X, Zhao Y-P. Atomic mechanisms and equation of state of methane adsorption in carbon nanopores. J Phys Chem C 2014;118:17737–44.
[17] Wang X, Huang X, Lin K, Zhao Y-P. The constructions and pyrolysis of 3D kerogen macromolecular models: experiments and simulations. Glob Challeng 2019;3:1900006.
[18] Wang X, Zhao Y-P. The time-temperature-maturity relationship: a chemical kinetic model of kerogen evolution based on a developed molecule-maturity index. Fuel 2020;278:118264.
[19] Yang N, Liu S, Yang X. Molecular simulation of preferential adsorption of CO_2 over CH_4 in Na-montmorillonite clay material. Appl Surf Sci 2015;356:1262–71.
[20] Wang Q, Li R. Research status of shale gas: a review. Renew Sustain Energy Rev 2017;74:715–20.
[21] Makaremi M, Jordan KD, Guthrie GD, Myshakin EM. Multiphase Monte Carlo and molecular dynamics simulations of water and CO_2 intercalation in montmorillonite and beidellite. J Phys Chem C 2015;119:15112–24.
[22] Kadoura A, Nair AKN, Sun S. Adsorption of carbon dioxide, methane, and their mixture by montmorillonite in the presence of water. Microporous Mesoporous Mater 2016;225:331–41.
[23] Huang X, Zhao Y-P, Wang X, Pan L. Adsorption-induced pore blocking and its mechanisms in nanoporous shale due to interactions with supercritical CO2. J Petrol Sci Eng 2019;178:74–81.
[24] Feng G, Kang Y, Sun Z-d, Wang X-c, Hu Y-q. Effects of supercritical CO2 adsorption on the mechanical characteristics and failure mechanisms of shale. Energy 2019;173:870–82.
[25] Yu H, Yuan J, Guo W, Cheng J, Hu Q. A preliminary laboratory experiment on coalbed methane displacement with carbon dioxide injection. Int J Coal Geol 2008;73:156–66.
[26] Middleton RS, Carey JW, Currier RP, Hyman JD, Kang Q, Karra S, Jiménez-Martínez J, Porter ML, Viswanathan HS. Shale gas and non-aqueous fracturing fluids: opportunities and challenges for supercritical CO2. Appl Energy 2015;147:500–9.
[27] Shi JQ, Durucan S. A bidisperse pore diffusion model for methane displacement desorption in coal by CO_2 injection. Fuel 2003;82:1219–29.
[28] Yuan Q, Zhu X, Lin K, Zhao Y-P. Molecular dynamics simulations of the enhanced recovery of confined methane with carbon dioxide. Phys Chem Chem Phys 2015;17:31887–93.
[29] Wu HA, Chen J, Liu H. Molecular dynamics simulations about adsorption and displacement of methane in carbon nanochannels. J Phys Chem C 2015;199:13652–7.
[30] Liang W, Zhang B, Han J. Experimental study on coal bed methane displacement and recovery by super critical carbon dioxide injection. J China Coal Soc 2014;39:1511–20.
[31] Zhang H, Cao D. Molecular simulation of displacement of shale gas by carbon dioxide at different geological depths. Chem Eng Sci 2016;156:121–7.
[32] Lin K, Yuan QZ, Zhao Y-P, Cheng CM. Which is the most efficient candidate for the recovery of confined methane: water, carbon dioxide or nitrogen? Extreme Mech Lett 2016;9:127–38.
[33] Hirano T. In: Stewart JJP, editor. MOPAC manual. seventh ed. 1993.